

Multiphoton ANS fluorescence microscopy as an *in vivo* sensor for protein misfolding stress

Kevin C. Hadley · Michael J. Borrelli ·
James R. Lepock · JoAnne McLaurin ·
Sidney E. Croul · Abhijit Guha · Avijit Chakrabartty

Received: 7 February 2011 / Revised: 23 March 2011 / Accepted: 24 March 2011 / Published online: 12 April 2011
© Cell Stress Society International 2011

Abstract The inability of cells to maintain protein folding homeostasis is implicated in the development of neurodegenerative diseases, malignant transformation, and aging. We find that multiphoton fluorescence imaging of 1-anilinonaphthalene-8-sulfonate (ANS) can be used to assess cellular responses to protein misfolding stresses. ANS is relatively nontoxic and enters live cells and cells or tissues fixed in formalin. In an animal model of Alzheimer's disease, ANS fluorescence imaging of brain tissue sections reveals the binding of ANS to fibrillar deposits of amyloid peptide (A β) in amyloid plaques and in cerebro-

vascular amyloid. ANS imaging also highlights non-amyloid deposits of glial fibrillary acidic protein in brain tumors. Cultured cells under normal growth conditions possess a number of ANS-binding structures. High levels of ANS fluorescence are associated with the endoplasmic reticulum (ER), Golgi, and lysosomes—regions of protein folding and degradation. Nuclei are virtually devoid of ANS binding sites. Additional ANS binding is triggered by hyperthermia, thermal lesioning, proteasome inhibition, and induction of ER stress. We also use multiphoton imaging of ANS binding to follow the *in vivo* recovery of cells from

James R. Lepock, deceased, 23 August 2005.

Electronic supplementary material The online version of this article (doi:10.1007/s12192-011-0266-6) contains supplementary material, which is available to authorized users.

K. C. Hadley · J. R. Lepock
Department of Medical Biophysics, University of Toronto,
Ontario Cancer Institute,
101 College Street,
Toronto, ON M5G 1L7, Canada

M. J. Borrelli
Department of Radiology,
University of Arkansas for Medical Sciences,
4301 W. Markham St.,
Little Rock, AR 72205, USA

J. McLaurin
Department of Laboratory Medicine and Pathobiology, Centre for
Research in Neurodegenerative Diseases, University of Toronto,
6 Queen's Park Cres. W.,
Toronto, ON M5S 3H2, Canada

S. E. Croul
Department of Laboratory Medicine and Pathobiology, University
of Toronto, UHN Path 11E426 Toronto General Hospital,
200 Elizabeth St.,
Toronto, ON M5G 2C4, Canada

A. Guha
Arthur and Sonia Labatt Brain Tumour Centre,
Hospital for Sick Children's Research Institute,
Toronto, ON M5G 1X8, Canada

A. Chakrabartty
Campbell Family Institute for Cancer Research,
Ontario Cancer Institute, University Health Network,
Toronto, ON, Canada

A. Chakrabartty
Department of Medical Biophysics, University of Toronto,
Toronto, ON, Canada

A. Chakrabartty
Department of Biochemistry, University of Toronto,
Toronto, ON, Canada

A. Chakrabartty (✉)
Toronto Medical Discovery Tower 4-307,
MaRS Center 101 College Street,
Toronto, ON M5G 1L7, Canada
e-mail: chakrab@uhnres.utoronto.ca

protein-damaging insults over time. We find that ANS fluorescence tracks with the binding of the molecular chaperone Hsp70 in compartments where Hsp70 is present. ANS highlights the sensitivity of specific cellular targets, including the nucleus and particularly the nucleolus, to thermal stress and proteasome inhibition. Multiphoton imaging of ANS binding should be a useful probe for monitoring protein misfolding stress in cells.

Keywords Protein homeostasis · Intracellular protein folding · Chaperones · Hsp70

Introduction

Cellular stress induced by protein misfolding is at the center of many human diseases. Several neurodegenerative disorders are caused by misfolding and aggregation of specific proteins, including α -synuclein in Parkinson's disease, SOD1 in familial amyotrophic lateral sclerosis, and huntingtin in Huntington's disease (Chiti and Dobson 2006). Mutations in CFTR and α_1 -antitrypsin cause the misfolding and accumulation of non-functional versions of these proteins, leading, respectively, to cystic fibrosis and α_1 -antitrypsin deficiency (Cheung and Deber 2008; Gregersen et al. 2006). More broadly, elevated burdens of unfolded intracellular protein—and increased stress on the networks that maintain protein homeostasis—are linked to malignant transformation and may lie at the foundation of human aging (Balch et al. 2008; Powers et al. 2009). Existing methods to measure protein misfolding stress rely on proxy biomarkers for protein folding, chaperone and proteasome function, but these measures generally require the introduction and expression of transgenes or are only suitable for endpoint analyses. We have found a novel application of a nontoxic small molecule which binds to intracellular targets and exhibits elevated fluorescence in response to protein-damaging cell stresses. In this paper, we employ multiphoton imaging of 1-anilino-8-naphthalenesulfonate (ANS) to noninvasively and quantitatively detect and signal changes in intracellular protein folding.

Fluorescent fusion proteins combining proteins of interest with green fluorescent protein (GFP) or related fluorophores can be expressed to directly track specific, individual disease-associated proteins. For example, GFP has been fused with α -synuclein (Unni et al. 2010) and huntingtin (Kotliarova et al. 2005) for in vivo investigation of cell culture and animal models of Parkinson's and Huntington's diseases. Misfolding of a particular protein can be linked to levels of expression, cellular or tissue localization, or to a portion of a cell or organism's life cycle. In most diseases, unfortunately, a single misfolding-prone protein has not been identified (and in most cases, probably does not exist) and a

broader approach to assessing the level of protein misfolding-driven cell stress is required.

Fluorescently labeled members of the heat shock protein family, including Hsp27 (Borrelli et al. 2002), Hsp70 (Zeng et al. 2004), and Hsp90 (Picard et al. 2006), have been widely used to study the response of these molecular chaperones to protein-damaging stressors in cells and model organisms. While these proteins are themselves resistant to damage, redistribution and binding of chaperone proteins indirectly reflects changes in the cellular burden of unfolded protein. Hsp70 (Sherman and Multhoff 2007), Hsp90 (Mahalingam et al. 2009), and endoplasmic reticulum (ER) stress proteins expressed as part of the unfolded protein response (UPR) (Moenner et al. 2007), have also all been implicated in buffering cancer cells and tumors from the stresses of malignancy, allowing tumors to proliferate. Several clinical trials now underway involve Hsp90 inhibitors as a novel approach to cancer treatment (Trepel et al. 2010); it would be useful to be able to directly monitor the effect of candidate drugs on protein misfolding stresses.

Refolding of thermally denatured luciferase (and concomitant recovery of bioluminescence activity) has been used as a functional measure of cellular chaperone activity (Nollen et al. 2001). Nonaka and Hasegawa (2009) recently reported using expression of GFP coupled to a degron (a short peptide which targets its protein for proteasomal degradation) to track the activity and function of the proteasome. While extremely powerful, techniques relying on fluorescent protein reporters require the transfection of cells and the expression of non-endogenous proteins that may affect the system under study. Developing stable expression systems can also be very time-consuming, particularly in the study of higher organisms.

Protein folding homeostasis may also be monitored through existing biochemical signaling pathways. For example, the UPR is activated under conditions of ER stress, triggering an assortment of signals. Phosphorylation of eIF2 α ; elevated expression of the proteins BiP, CHOP, HSPA5, and DVE-1; cleavage and activation of the transcription factor ATF-6 α ; and splicing of XBP1 mRNA are all recognized markers for UPR activation (Lin et al. 2008), and detection of these markers can serve as an indirect sensor for the accumulation of misfolded proteins. Unfortunately, the detection of endogenous proteins or nucleic acids generally requires solubilization (for blotting or PCR of cell lysates) or fixation (for immunohistochemistry or immunofluorescence) of the cell, preventing the tracking of these markers over time in individual live cells. All of these measures are proxies for the presence or quantity of misfolded protein, and many rely on the presence and proper function of specific intracellular signaling pathways.

We believe that ANS imaged by multiphoton fluorescence microscopy is a probe that is broadly sensitive to the

stresses of protein misfolding *in vivo*. It is relatively nontoxic and can enter all compartments of living cells, thereby avoiding transfection or other direct modifications of the cell's biology. ANS has a long history of *in vitro* use for the study of isolated biomolecules and simple molecular systems in cuvette-based assays. This small molecule is essentially non-fluorescent in aqueous solution, but its fluorescence quantum yield increases several hundredfold in a hydrophobic environment. In practice, this means that ANS becomes highly fluorescent when embedded in exposed hydrophobic pockets of proteins in partly folded or "molten globule" states (Semisotnov et al. 1991; Slavík 1982). Historically, ANS has been unsuited to live-cell imaging applications by epifluorescence microscopy, as it is an ultraviolet-excited dye. It binds strongly to serum albumin, generating an overwhelming background fluorescence under normal mammalian cell culture conditions. Each cell contains a very large number of potential ANS binding sites, and previous attempts to use ANS in epifluorescence microscopy were largely unsuccessful (Dyckman and Weltman 1970; Finegold et al. 1974; Witz et al. 1973).

The introduction of multiphoton microscopy opens the door to imaging intracellular ANS fluorescence. Multiphoton excitation (MPE) of ANS is confined to the focal plane of the microscope's objective lens, suppressing out-of-focus fluorescence and giving confocal-like optical sectioning. Because MPE employs near-infrared light, concerns about phototoxicity are greatly reduced (Denk et al. 1990; König 2000). With this new tool, we are able to directly image ANS binding sites in living cells.

Materials and methods

Cell culture HeLa S3 cells (ATCC, Manassas, VA) were cultured in plastic T25 culture flasks (Nalge Nunc, Rochester, NY) in DMEM H21/Ham F12 1:1 medium (DMEM/F12) supplemented with 10% fetal bovine serum (FBS, Invitrogen, Carlsbad, CA).

Fluorimetry A Photon Technology International (London, ON) fluorimeter was used for *in vitro* measurements. Excitation was at 375 nm, excitation and emission bandpass of 2 nm. Emission spectra were collected in 50 μ M of ANS. Bovine serum albumin (Fisher Scientific, Pittsburgh, PA) was dissolved in phosphate-buffered saline (PBS) to a concentration of 1 mg/mL. β -Amyloid 1–42 (A β 42, gift of Pharhad Eli Arslan) was diluted into 150 mM NaCl plus 10 mM phosphate buffered to pH 6.0 or pH 8.0 and incubated at 37°C for 3 h; ANS was added 30 min prior to fluorimetry. Total lipids were collected from HeLa cells by extraction in chloroform/methanol (Folch et al. 1957). Polar lipids were isolated by

precipitation with ice-cold acetone (Choquet et al. 1992), pelleted by centrifugation, and redissolved in chloroform.

To prepare unilamellar vesicles, chloroform solutions of DOPG (1,2-Dioleoyl-*sn*-Glycero-3-[Phospho-*rac*-(1-glycerol)]) (Avanti Polar Lipids, Alabaster, AL) or isolated polar lipids were dried overnight under vacuum, then resuspended in PBS by repeated freezing and thawing. Small unilamellar vesicles were generated by sonication in a glass test tube in a Branson 1210 bath sonicator (Branson Ultrasonic, Danbury, CT) until the cloudy suspension took on a "pearly" appearance (approximately 30 min).

Cell survival assays 3×10^4 HeLa cells per well were seeded on 96-well clear-bottom polystyrene tissue culture-treated plates (Corning Life Sciences, Corning, NY) and incubated in DMEM/F12 for 24 h. At 24 or 6 h prior to fixation, fresh growth medium supplemented with phosphate-buffered ANS (8-anilino-1-naphthalenesulfonic acid) at concentrations ranging from 0 to 1,000 μ M, 50 μ M melittin or 0 to 100 μ M MG132 (all Sigma-Aldrich, St. Louis, MO) was added to the cells. The cells were fixed at 4°C using 10% trichloroacetic acid, and cell survival was measured using the sulforhodamine B assay as described (Skehan et al. 1990).

Microscopy Images were collected using a Zeiss (Oberkochen, Germany) LSM 510 META confocal microscope. High-resolution images employed a 1.2 numerical aperture (NA) $\times 40$ water immersion objective; lower magnification fields were collected with a 0.75-NA $\times 20$ air objective. While ANS fluorescence was measured using two-photon excitation (see below), all other fluorescence images were collected in confocal mode. The photomultiplier tube voltages were adjusted for each imaging session to make full use of the available dynamic range; no adjustments were made between control and treatment images. The live cells were plated onto Lab-Tek chambered #1.0 borosilicate coverglasses (Nalge Nunc) and allowed to recover for at least 24 h prior to imaging. The live cells were maintained during the imaging in CO₂ Independent Medium (Invitrogen) supplemented with 10% FBS. An enclosed, heated stage (Zeiss) and Tempcontrol 37 objective heater (PeCon, Erbach, Germany) were used to maintain cells at a constant temperature.

ANS fluorescence imaging A stock solution of 10 mM ANS in PBS at pH 7.4 was used for preparing all working solutions. Prewarmed CO₂ Independent Medium supplemented with 250 μ M ANS was added to the cells at least 1 h prior to imaging. Two-photon ANS fluorescence was excited using a Chameleon tunable infrared laser (Coherent, Santa Clara, CA) at 750 nm. ANS fluorescence was imaged using a 435–485-nm band-pass filter.

Murine amyloid plaques Transgenic CRND8 mice express a mutant form of the human amyloid precursor protein under the brain-specific PrP promoter (Chishti et al. 2001). The transgenic mice and their nontransgenic littermates were sacrificed and their brains were fixed in phosphate-buffered formalin. Twenty-micrometer cryosections were cut onto glass slides and stained with 1% thioflavin S (ThS, Sigma) (Hawkes and McLaurin 2009) or 10 μM ANS in PBS and sealed under a coverslip for imaging. ThS fluorescence was excited at 488 nm and detected through 505-nm longpass filter.

Human brain tumor sections Surgically excised brain tissue was snap frozen in liquid nitrogen and archived at -80°C by the Canadian Virtual Brain Tumour Bank (Toronto Western Hospital, Toronto, ON). Cryostat sections from banked tissue were cut on glass slides and postfixed in 4% formaldehyde in PBS. ANS-stained sections were equilibrated in 50 μM ANS in PBS and coverslipped under 50 μM ANS in phosphate-buffered glycerol mountant. Adjacent sections were stained with hematoxylin and eosin, and transmitted light images were collected using the $\times 40$ objective of an Aperio ScanScope XT (Aperio Technologies, Vista, CA).

Organelle labelling BODIPY FL C_5 -ceramide, ER Tracker Green, MitoTracker Orange CMTMRos, and LysoTracker Green DND-26 (Molecular Probes, Carlsbad, CA) were prepared and used according to the manufacturer's directions. Neutral lipid droplets were labeled using Nile red (Greenspan et al. 1985) (Eastman Kodak, Rochester, NY). Excitation wavelength and emission filter sets were as follows: BODIPY FL C_5 -ceramide, 488 nm (excitation)/560-nm longpass (red excimer emission); ER Tracker, 488 nm/505-nm longpass; MitoTracker, 543 nm/565–615-nm bandpass; LysoTracker, 488 nm/505-nm longpass; and Nile red, 488 nm/500–550-nm bandpass (gold fluorescence).

Transfection and YFP fluorescence imaging Plasmids containing the cDNA for human Hsp70 fused to yellow fluorescent protein (YFP) or YFP alone, were transfected into HeLa cells using a BTX ECM 830 electroporator (Harvard Apparatus, Holliston, MA) (Tupling et al. 2004; Wu et al. 1985). Cells were cultured on chambered coverslips as described above. YFP fluorescence was excited at 514 nm and imaged using a 535–590-nm bandpass filter.

Lesion creation Linear thermal lesions were created using the 750-nm infrared laser at high power (approximately 250 mW at the microscope objective). The beam was scanned across the sample using the LSM 510's region of interest photobleaching tool. A one-pixel-high rectangle was selected and was "bleached" 50 times.

Hyperthermia treatment and proteasome inhibition Chambered coverslips were sealed with Parafilm M and immersed in a $43.0 \pm 0.1^{\circ}\text{C}$ water bath for 15 to 30 min as indicated. The medium was additionally supplemented with 5 μM MG132 for tests involving proteasome inhibition.

Fluorescence recovery after photobleaching Cells expressing YFP alone or the Hsp70-YFP fusion protein were cultured on chambered coverslips and were heat-shocked as described. Regions of interest (ROI) were identified as nuclear or cytoplasmic by visual inspection of the fluorescence and differential interference contrast (DIC) images. The fluorescence recovery after photobleaching (FRAP) experiments were conducted in confocal mode, with the pinhole set to approximately 1.2 Airy units diameter (nominal optical slice thickness 1.0 μm). Fluorescence intensity was sampled at 1.5- μs intervals using the LSM 510's spot imaging mode; 1,000 measurements were averaged to generate a raw dataset with 1.5 ms resolution. Five measurements were collected prior to photobleaching and averaged to determine the initial fluorescence of the ROI. The bleaching pulse was 3-ms long; fluorescence was followed for at least 300 ms (greater than ten times the recovery time constant) to allow for complete recovery of the freely diffusing population of fluorescent protein.

The fluorescence recovery curve was fitted with a first-order exponential recovery using Origin 4.1 (Microcal Software, Northampton, MA) to extract estimates for the minimum fluorescence immediately following bleaching and for the final fluorescence after recovery. The unbound or mobile fraction was deemed equal to the net amount of fluorescence recovered divided by the net amount of fluorescence bleached.

Tunicamycin treatment HeLa cells were cultured on chambered coverslips. The regular growth medium was supplemented with tunicamycin (Sigma) at concentrations ranging from 0 to 20 $\mu\text{g}/\text{mL}$, doses sufficient to trigger the UPR (Delom et al. 2007; Hazel et al. 1999). At 3 h, the cells were washed briefly with PBS and fixed with phosphate-buffered 2% paraformaldehyde. The cells were stained and imaged under 50 μM of ANS in PBS. Z stacks of images were collected at 1- μm intervals through the entire thickness of the cell monolayer. A uniform, low intensity threshold (20 units, out of the full scale of 255) was used to eliminate all non-cellular background fluorescence, and the average fluorescence intensity over the remaining volume was calculated. The mean of five such measurements was taken for each tunicamycin concentration; the resulting dose–response was fitted and normalized using the four-parameter logistic (Hill slope) equation.

Fig. 1 a In cuvette fluorescence measurements of ANS with equal mass concentrations of *A*, aggregated fibrillar A β 42 at pH 6.0; *B*, vesicles of isolated cellular polar lipids from HeLa cells; *C*, soluble, monomeric A β 42 at pH 8.0; and *D*, DOPG vesicles. **b** Widefield images of murine brain with amyloid deposits stained with ANS or **c** thioflavin S; *scale bar*, 50 μ m. **d**, **e** Enlargements of dense plaques and **f**, **g** cerebrovascular amyloid deposits; *scale bar*, 10 μ m. Human pilocytic astrocytoma sections exhibiting Rosenthal fibers, stained with **h** hematoxylin and eosin or **i** ANS; *scale bar*, 50 μ m

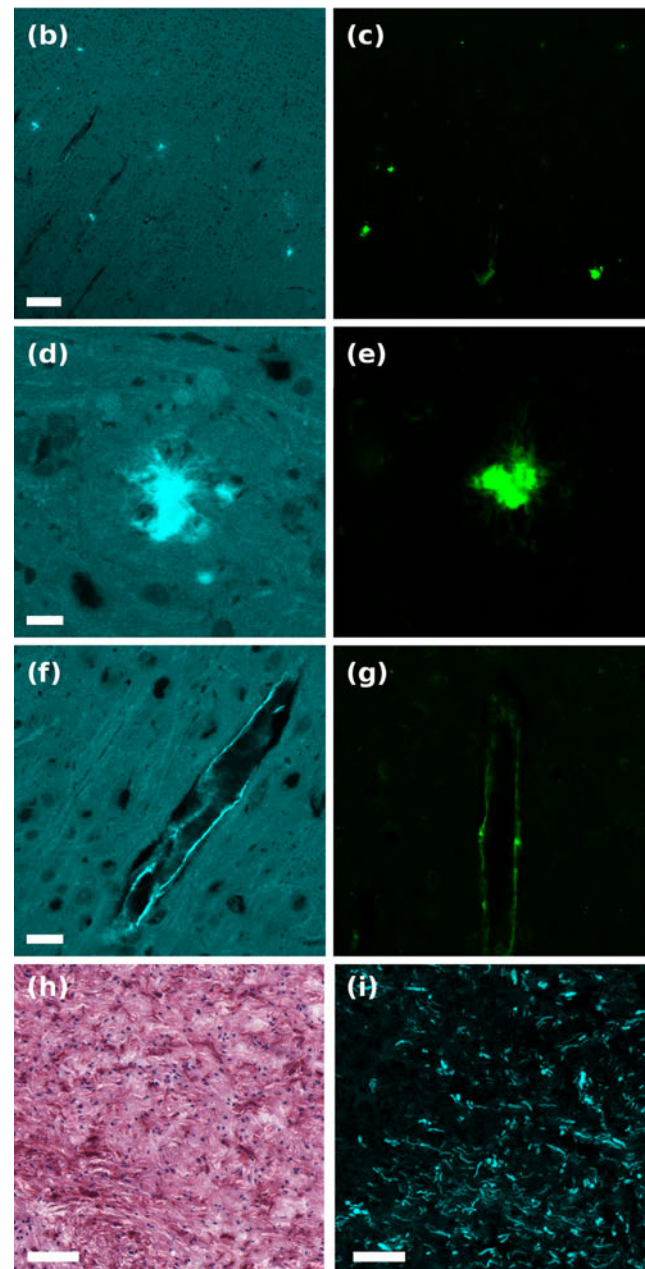
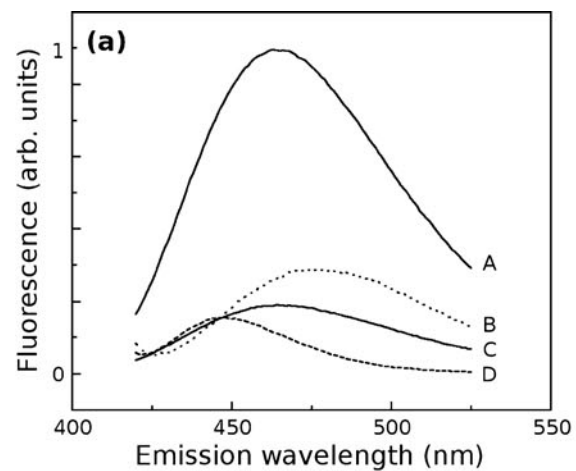
Image processing All image processing was performed using ImageJ version 1.30v and later (NIH, Bethesda, MD). Where brightness and contrast have been adjusted for display, identical settings were used for experimental and control images. No gamma or other nonlinear adjustments were made to any image, and all image quantification used the raw, unprocessed images.

Results

ANS fluoresces in the presence of misfolded protein in vitro and in tissue

ANS has been extensively used as an in vitro probe of protein conformation; elevated ANS binding and fluorescence is associated with “molten globule” protein conformational states and the accompanying formation and exposure of hydrophobic binding pockets (Semisotnov et al. 1991). The fluorescence emission spectra of equal mass concentrations of A β 42 or lipid vesicles in solution with ANS are shown in Fig. 1a. At pH 8.0, A β exists as a stable, unstructured, soluble species, and shows low fluorescence in the presence of ANS (curve C). In contrast, A β 42 at pH 6.0 misfolds into amyloid fibrils (Barrow and Zagorski 1991) and shows a much greater degree of ANS binding and fluorescence (curve A). The fluorescence of ANS bound to misfolded A β 42 is significantly higher than ANS bound to unstructured soluble A β 42 or lipid bilayers prepared from polar lipids (glycolipids and phospholipids) extracted from HeLa cells (Fig. 1a, curve B) or from synthetic phospholipid (Fig. 1a, curve D).

We wondered whether this vivid response might also occur in the more complex environment of mammalian tissue. Figure 1b shows a section of transgenic CRND8 mouse brain stained with ANS and imaged by two-photon microscopy. Another section from the same brain is shown stained with thioflavin S (ThS, Fig. 1c), a widely used fluorescent probe specific for amyloid deposits (Kelényi 1967). Visible in both figures are dense plaques as well as extended patches of cerebrovascular amyloid lining blood vessels (enlarged in Fig. 1f, g). At high magnification (Fig. 1d, e), the amyloid plaques are vividly fluorescent.



ANS also appears to be sensitive to non-amyloid deposits of aggregated protein that are not detected by thioflavin S. Figure 1 also shows sections of a low-grade (WHO grade I) pilocytic astrocytoma stained with hematoxylin (Fig. 1h) and eosin (H&E) or ANS (Fig. 1i). Detectable by H&E are eosinophilic deep red Rosenthal fibers, a common feature of low-grade human brain tumors. They consist of bundles of insoluble, non-amyloid aggregates of intermediate filament protein (glial fibrillary acidic protein or GFAP) (Wippold et al. 2006). The Rosenthal fibers are intensely fluorescent with ANS demonstrating that non-amyloid misfolded structures can also be illuminated by ANS.

While ANS fluorescence in the tissue sections was by far the most intense within the amyloid plaques and non-amyloid Rosenthal fibers, we observed some fluorescence from the surrounding tissue that exhibited normal morphology. Because there was no conspicuous pathology associated with this other tissue, this finding prompted us to investigate what non-pathological intracellular structures might also bind ANS.

Intracellular ANS fluorescence colocalizes with sites of protein synthesis and degradation

Using two-photon microscopy, it is possible for the first time to conduct a high-resolution survey of ANS fluorescence in living cells. When ANS is added to cell culture medium, it crosses the plasma membrane and the cells equilibrate with ANS in solution within minutes (typically 45 min is sufficient for equilibration). Figure 2a shows a two-photon image of ANS fluorescence in a living HeLa cell; the inset shows the corresponding DIC transmitted light image. The most conspicuous feature of the cell is the near absence of ANS fluorescence in the cell nucleus. The perimeter of the cell does not show elevated fluorescence, suggesting that the plasma membrane is not a major source of ANS fluorescence. The inherent toxicity of ANS in HeLa cells is low (Fig. 2b). Cells are amply fluorescent at ANS concentrations of 250 μM and above, but this concentration does not significantly affect cell survival or growth even after exposures of at least 24 h. Concentrations as high as 0.5 mM are well-tolerated for exposures of at least 6 h. A significant fraction of the ANS is bound to soluble serum albumin in the culture medium; we found that much lower ANS concentrations are sufficient to stain cells (and tissues) under serum-free conditions.

We sought to identify the major sites of intracellular ANS binding in unstressed HeLa cells using a variety of fluorescent organelle probes (Fig. 3). Strong colocalization was observed throughout the cell between ANS fluorescence and a probe for the endoplasmic reticulum (Fig. 3a, f). Bright ANS fluorescence was also observed in the Golgi (Fig. 3b, g). These organelles are associated with

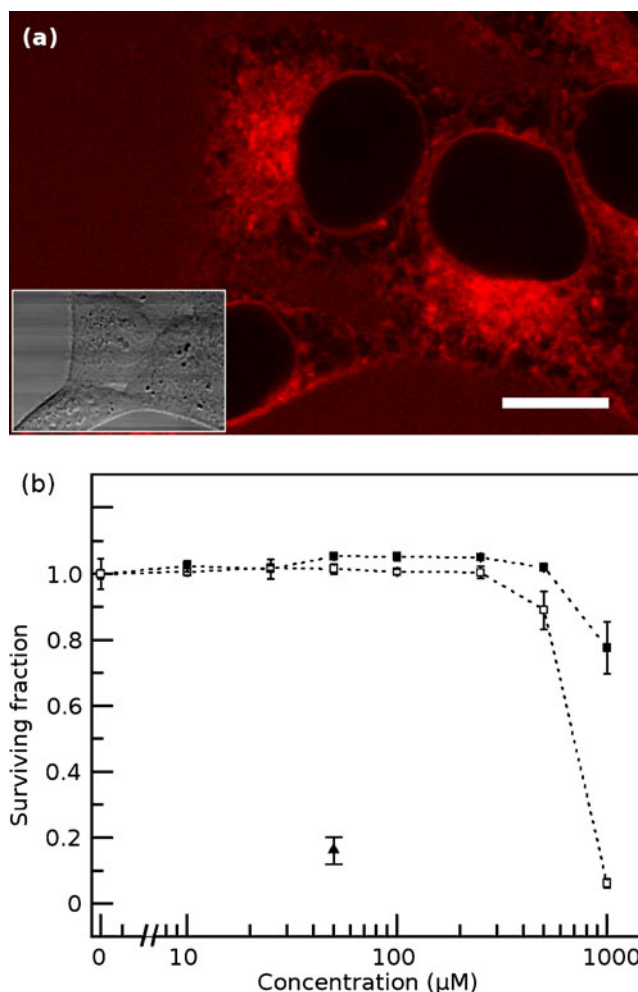


Fig. 2 **a** Living HeLa cell stained with ANS under normal growth conditions. The cell nucleus is clear of ANS fluorescence. Vivid fluorescence is observed adjacent to the nucleus while regions of both diffuse and punctate ANS fluorescence are seen throughout the cytoplasm. The plasma membrane is not noticeably fluorescent compared to the cytoplasm. The area around the cell exhibits a uniform low level of fluorescence primarily due to the binding of ANS to serum proteins in the culture medium. *Scale bar*, 10 μm . *Inset* shows the same region by DIC. **b** ANS is not toxic to living cells at the concentrations used for imaging. Cell survival, as measured using a sulforhodamine B assay, was not significantly impaired at 6 h (*black squares*) or 24 h (*white squares*) of exposure to concentrations of ANS up to 250 μM in culture medium. Cells were also treated with 50 μM melittin (*black triangle*), a cytotoxin, for 6 h as a positive control for cell death

the translation, folding, and/or packaging of cellular proteins. A fraction of cytoplasmic proteasomes are also coupled to the cytosolic face of the ER, where they are involved in ER-associated degradation of protein (ERAD) (Wójcik and DeMartino 2003; Brodsky and McCracken 1999).

Fluorescence of the lysosomal probe LysoTracker Green colocalized with brightly ANS-fluorescent cytoplasmic punctae (Fig. 3c, h). Lysosomes have a low pH, promoting non-native protein conformational states, and are a site of intracellular protein degradation.

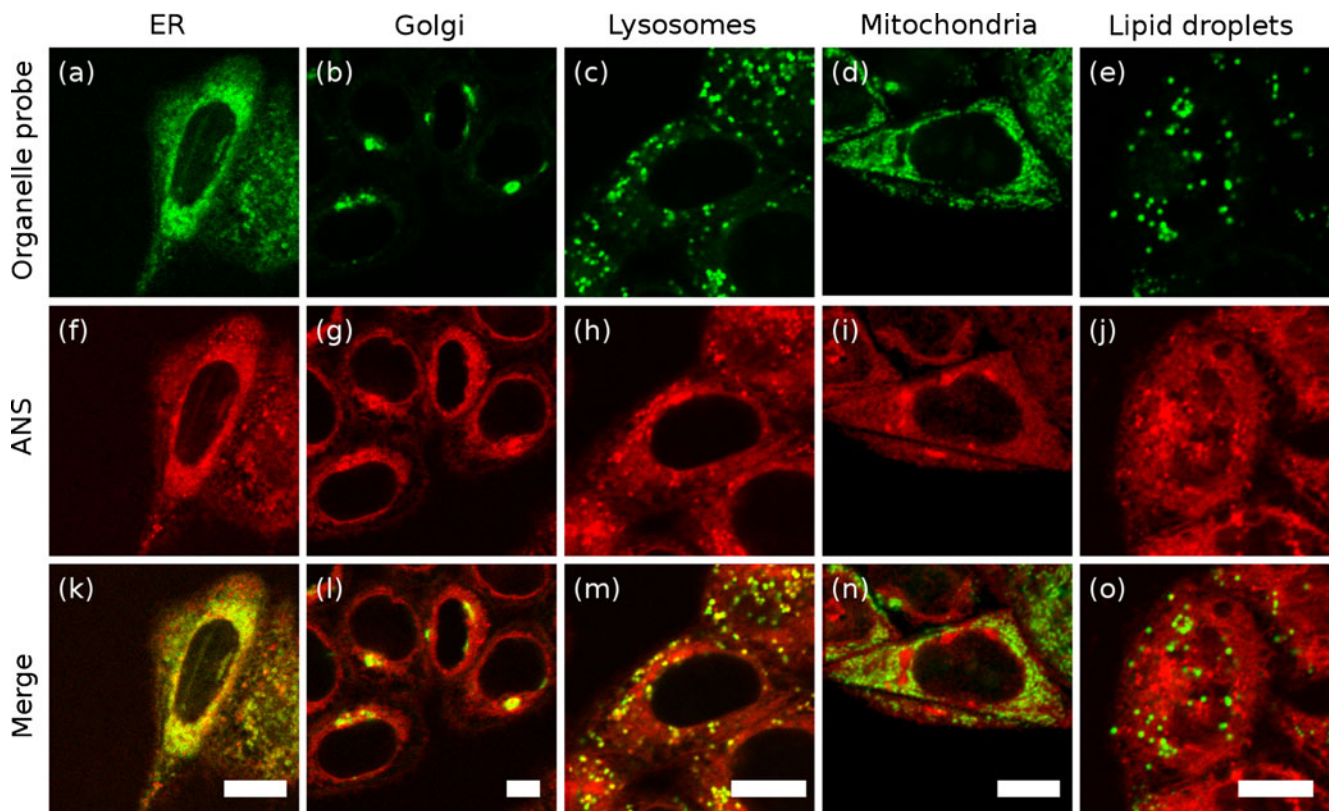


Fig. 3 Colocalization of ANS with organelle probes *in vivo*. Organelle probes (a–e), ANS fluorescence (f–j), overlay (k–o). Probes: ER Tracker Green (a, endoplasmic reticulum), BODIPY FL C₅-ceramide (b, Golgi apparatus), LysoTracker Green (c, lysosomes), MitoTracker Orange (d, mitochondria), Nile Red (e, intracellular lipid droplets).

Scale bars, 10 μ m. Strong overlap of organelle markers with ANS fluorescence is observed for the endoplasmic reticulum, Golgi, and lysosomes. Poor overlap is noted for the mitochondria, the nucleus, and intracellular neutral lipids

In contrast, fluorescence of ANS did not colocalize with a mitochondrial probe (Fig. 3d, i), nor with intracellular neutral lipid droplets (Fig. 3e, j). By comparison of ANS fluorescence with transmitted light images (inset Fig. 2a), ANS fluorescence is also not present within the cell nucleus nor does fluorescence appear elevated near the plasma membrane. We expect that there would be interactions between ANS and some well-folded cellular proteins that have exposed hydrophobic binding pockets (Slavík 1982). However, our results indicate that ANS fluorescence is predominantly associated with organelles expected to contain proteins in non-native conformations.

Curves D and B from Fig. 1a are from small unilamellar vesicles generated using either pure DOPG or polar lipids isolated from cultured HeLa cells, respectively. In both cases, the ANS fluorescence associated with these lipid vesicles is relatively modest. Coupled with the low apparent fluorescence of the plasma membrane, we believe that the contribution of lipid membranes themselves to cellular ANS fluorescence is low; however, there may be a finite contribution from membrane proteins. As membrane lipid composition varies between organelles and the plasma membrane, the intrinsic fluorescence of cellular membranes may also vary.

Intracellular ANS fluorescence tracks with Hsp70 recruitment

Thermal lesioning To examine the binding and fluorescence of ANS in the presence of a nonspecific population of misfolded protein, we prepared cells expressing the chaperone Hsp70 fused to yellow fluorescent protein (Hsp70-YFP) under a constitutive promoter. Hsp70 is known to reversibly bind to short stretches of hydrophobic residues (typically a leucine flanked by two or three other hydrophobic residues (Fourie et al. 1994)) exposed during *de novo* protein synthesis or made accessible by stress-induced misfolding. Hsp70 is normally a soluble protein that shuttles between the cytoplasm and nucleus but can be temporarily immobilized if it is bound to an insoluble protein partner or aggregate. Under normal growth conditions, Hsp70-YFP is predominantly cytoplasmic, but still detectable within the nucleus (Fig. 4d).

We created a narrow, linear, thermal lesion across the cytoplasm and nucleus using an infrared laser, rapidly generating and precipitating a local pool of misfolded protein. Within less than 1 min, Hsp70-YFP fluorescence accumulated along the length of the lesion within the cell

Fig. 4 HeLa cells are shown before (a, d) or after (b, c, e, f) linear thermal lesions were created using an infrared laser. ANS (b, c) bound immediately to the lesion site. YFP-conjugated Hsp70 was also rapidly recruited to the lesion (e), but YFP expressed on its own (f) was not. Scale bars, 10 μm

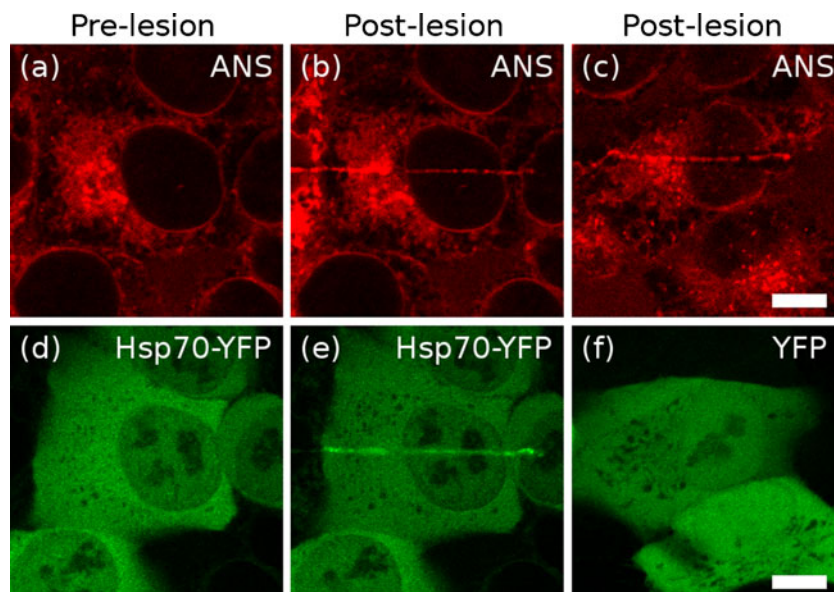


(Fig. 4e). ANS fluorescence simultaneously appeared in the same location (Fig. 4b). In control cells expressing YFP alone (unconjugated to a chaperone, Fig. 4f), ANS fluorescence was still recruited to the lesion site; however, no YFP accumulation occurred. We therefore believe that we are generating a misfolded protein that specifically binds the Hsp70 chaperone, while simultaneously detecting this damaged protein using ANS.

Hyperthermia Nonlethal heat shock drives a dramatic translocation of Hsp70. Its nucleocytoplasmic distribution is reversed, and the nuclear concentration of Hsp70—particularly near the nucleolus—becomes quite high (Alastalo et al. 2003; Welch and Feramisco 1984). We also observe a similar pattern of nuclear accumulation with our Hsp70-YFP (Supplementary Fig. S3a, b, nucleoli identified by arrowheads). The Hsp70-YFP in all heat-shocked cell nuclei takes on a mottled, punctate appearance, and some cells show conspicuous accumulation of Hsp70-YFP in or around nucleoli. We noted some cell-to-cell variation in the level of Hsp70-YFP expression that may be due to the transient transfection. The images shown in Supplementary Fig. S3a, b are representative of the control and heat-shocked cells that we observed.

In addition to this accumulation of Hsp70 in the nuclear compartment, there is also a significant reduction in the freely diffusing population of this chaperone (previously observed by Zeng et al. (2004)). We used FRAP to quantify the immobile, bound fraction of Hsp70-YFP in living HeLa cells. We did not attempt to segment the nucleus or cytoplasm into subcompartments for FRAP measurements, or to select (or reject) cells with particularly high or low levels of nucleolar fluorescence. Under control conditions, the fraction of Hsp70 that is immobile is 0.19 ± 0.06 (mean \pm SD)

in the cytosol and 0.24 ± 0.05 in the nucleus. After a significant but nonlethal heat shock (43°C for 30 min), the bound or interacting fraction in the cytoplasm increases modestly to 0.27 ± 0.12 . In the nucleus, however, a very dramatic shift in Hsp70 binding occurs, where the interacting fraction rises to 0.64 ± 0.12 . A stable, non-interacting control protein (YFP alone) showed a very small interacting fraction (between 0.05 and 0.07) that was unaffected by hyperthermia treatment in both nuclear and cytoplasmic compartments (Supplementary Fig. S3f–i).

Hyperthermia treatment leads to the generation of nuclear Hsp70 interaction sites. These sites are presumably thermally misfolded proteins. Given the property of ANS to bind misfolded proteins, we compared the generation of Hsp70 binding sites with that of ANS binding sites after hyperthermia treatment. Comparing HeLa cells before (Fig. 5a) and 5 min after (Fig. 5b) a 15-min hyperthermia treatment, we observed an increase in nuclear ANS fluorescence, along with a prominent ANS fluorescence in the nucleoli. The accumulation of nuclear ANS fluorescence mirrored the nuclear accumulation of Hsp70 (Supplementary Fig. S3a, b). Autofluorescence makes a negligible contribution to apparent fluorescence under these imaging conditions; control cells not stained with ANS showed barely detectable autofluorescence that was unchanged by hyperthermia exposure (Supplementary Fig. S2).

Figure 5c plots the normalized ANS fluorescence of cell nuclei and whole cells before and after hyperthermia on the left-hand axis, following the recovery of cells for 100 min after their return to 37°C . The overall ANS fluorescence of the cells was slightly elevated by hyperthermia ($6 \pm 2\%$), but the cell nucleus showed a much more dramatic relative increase, up to $66 \pm 10\%$ above baseline. There are several

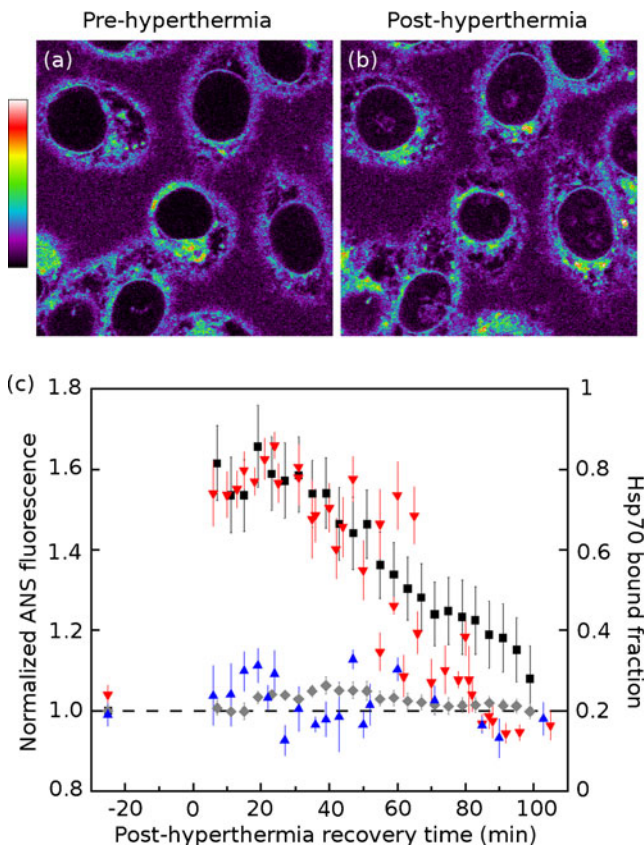


Fig. 5 Nuclear ANS fluorescence tracks with binding of Hsp70 chaperone in heat-shocked cells. HeLa cells **a** before and **b** immediately after a 15-min, 43°C heat shock. Following hyperthermia exposure, nuclei (especially nucleoli) exhibit elevated ANS fluorescence. **c** ANS fluorescence (left axis) for cell nuclei (*black square*) and whole cells (*gray diamond*) before, and during recovery from, hyperthermia exposure. Fluorescence values were normalized to prehyperthermia baseline. Overlaid is the bound Hsp70 fraction (right axis) measured by FRAP in nuclear (*red down-pointing triangle*) and cytoplasmic (*blue triangle*) compartments. The relative response to hyperthermia exposure is much greater in the nucleus than in the rest of the cells. Recovery of the cells (indicated by the return of Hsp70 binding and ANS fluorescence to near baseline levels) takes approximately 90 min and occurs in parallel by both measures

potential interpretations of this noteworthy difference between nuclear and whole cell ANS fluorescence changes. First, thermolabile proteins may be more abundant in the nucleus than in the cytoplasm. Second, thermolabile proteins in the nucleus may be more likely to form “molten globule” folding intermediates which have a particularly high affinity for ANS, whereas their cytoplasmic thermolabile proteins may tend to assume more extended unfolded states that do not bind ANS as effectively. Third, the high baseline level of ANS fluorescence associated with extra-nuclear organelles (the ER, Golgi, and lysosomes) may simply mask the increase in cytoplasmic ANS binding caused by hyperthermia.

Plotted on the right-hand axis of Fig. 5c is the immobile fraction of Hsp70-YFP, measured in the cytoplasm and the

nucleus. The elevated ANS fluorescence in the nucleus appears to track with the elevated level of Hsp70 binding. We interpret the local increases in ANS fluorescence (compared to control conditions) as representative of an elevated local burden of unfolded protein; regions of the cell showing an increased fluorescence in response to stress may represent sites of protein misfolding and processing. This suggests that the nuclear accumulation of Hsp70 in response to heat shock is driven by an immobilization and sequestration of chaperone from the soluble, nucleocytoplasmic shuttling pool of Hsp70. As thermally damaged nuclear proteins are refolded or degraded, ANS fluorescence and Hsp70 binding decline in tandem.

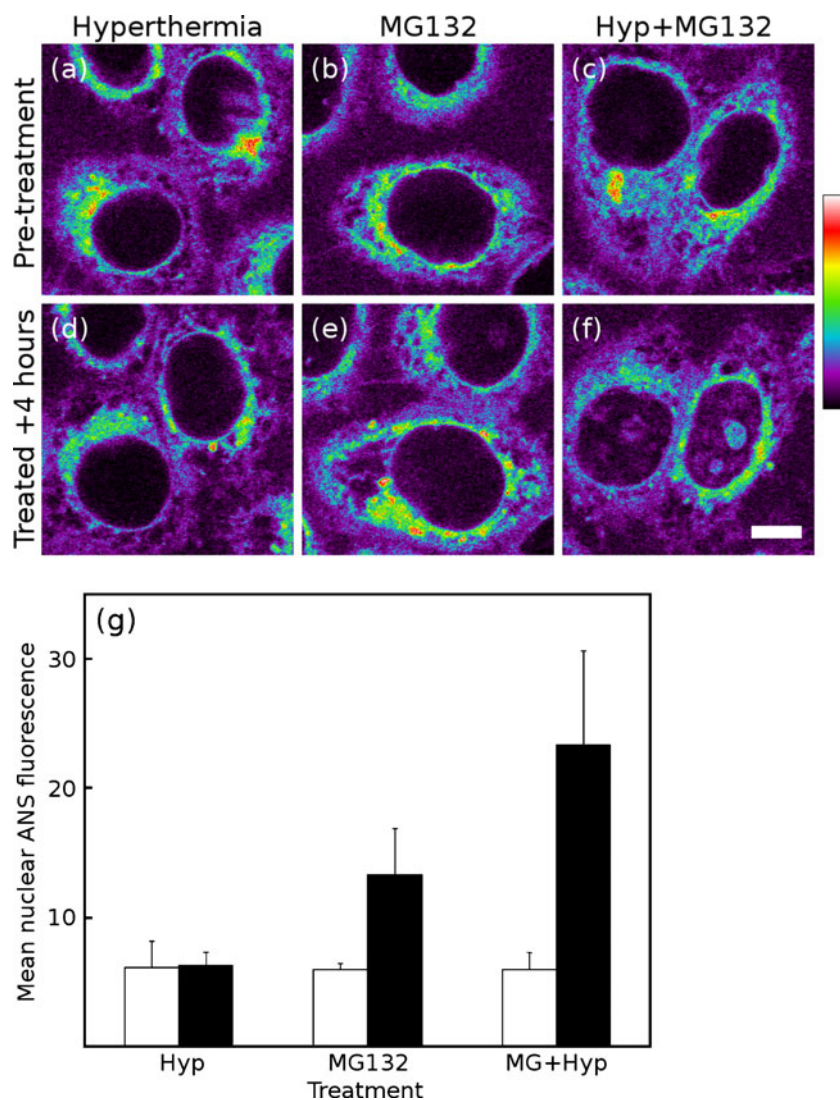
ANS fluorescence increases in response to proteasome inhibition, ER stress

Proteasome inhibition Figure 6a shows HeLa cells before a substantial, 30-min 43°C hyperthermia exposure; Fig. 6d shows the same cells after they have been allowed to recover for 4 h. The measurement of the mean nuclear fluorescence before the treatment and after recovery is shown in Fig. 6g; as seen by ANS fluorescence, the cells completely recover from this treatment. Figure 6b, e shows cells before and after a 4-h treatment with the proteasome inhibitor MG132. While MG132 does not directly damage proteins within the nucleus or nucleoli, impaired proteasomal degradation of proteins has an impact throughout the cell. The additional nuclear and nucleolar ANS fluorescence following MG132 treatment is a consequence of a pancellular increase in the unfolded protein burden.

Furthermore, MG132 treatment abrogates the recovery of cell nuclei following hyperthermia (Fig. 6c, f). Four hours after hyperthermia exposure coupled with proteasome inhibition, the cell nuclei (and especially nucleoli) remain brightly fluorescent by ANS imaging (Fig. 6g). The level of nuclear fluorescence seen in MG132-treated cells is higher with hyperthermia than without, reflecting the effect of introducing a large pool of thermally denatured protein to the cell.

ER stress response HeLa cells were cultured and treated with tunicamycin for 3 h. Tunicamycin inhibits the N-linked glycosylation of the membrane-targeted proteins, causing them to accumulate in the ER; by this mechanism it is a potent trigger of the unfolded protein response (Hiss et al. 2007). Figure 7 shows cells fixed with formaldehyde and stained with ANS, with 0 µg/mL (Fig. 7a) and 20 µg/mL (Fig. 7b) of tunicamycin. Buffered formaldehyde is a cross-linking fixative that appears to adequately preserve the conformation

Fig. 6 Proteasome inhibition impairs maintenance of nuclear proteins. Living HeLa cells were imaged before (**a–c**, *open bars* in **g**) and 4 h after (**d–f**, *solid bars* in **g**) the start of one of three treatments: 30-min 43°C hyperthermia (**a**, **d**); proteasome inhibition with 5 μ M MG132 (**b**, **e**); or hyperthermia with proteasome inhibition (**c**, **f**). Values shown indicate the mean nuclear fluorescence of at least five cells in each sample. Proteasome inhibition causes an accumulation of misfolded protein within the cell (**e**) and impairs the ability of a cell to recover from heat shock (**f**). *Scale bar*, 10 μ m. Quantification of mean nuclear fluorescence (**g**)



of cellular protein for the purposes of ANS imaging. A lower concentration of ANS (50 μ M) is required for imaging fixed cells in phosphate buffer because there is no serum albumin in the surrounding medium to bind the dye. Fixation allowed us to image large volumes of cells as they appeared at a single time point after tunicamycin treatment and to carry out all drug treatment and staining steps in parallel in order to minimize sample-to-sample handling differences.

Figure 7c plots the mean fluorescence intensity of ANS-stained cells as a function of tunicamycin concentration. ANS fluorescence follows tunicamycin concentration in a dose-dependent manner (the EC₅₀ for tunicamycin-driven activation of the UPR is reported to be 12 μ g/mL in cervical cancer cells (Delom et al. 2007)). We were not able to assess the effect of tunicamycin concentrations above 20 μ g/mL on ANS fluorescence; at very high doses, acute tunicamycin toxicity caused cells to detach from the plates before they could be fixed and imaged.

Discussion

We have demonstrated that ANS is nontoxic and capable of rapidly entering and equilibrating with living cells. In vitro, ANS has a high binding affinity for a subset of cellular proteins compared to non-protein cellular components (Slavík 1982). In vivo, ANS is readily imaged by multiphoton microscopy. We found that high intracellular ANS fluorescence is associated with organelles involved in protein synthesis, processing, and degradation. In tissue, particularly intense ANS fluorescence is observed from the aggregated protein within amyloid plaques, and within non-amyloid Rosenthal fibers.

ANS is a very general probe that interacts with a wide variety of protein (and some non-protein) targets. All living cells will exhibit a certain normal, baseline level of ANS binding affinity, reflecting interactions both with endogenous, well-folded proteins containing ANS binding sites and with incompletely folded or misfolded products of

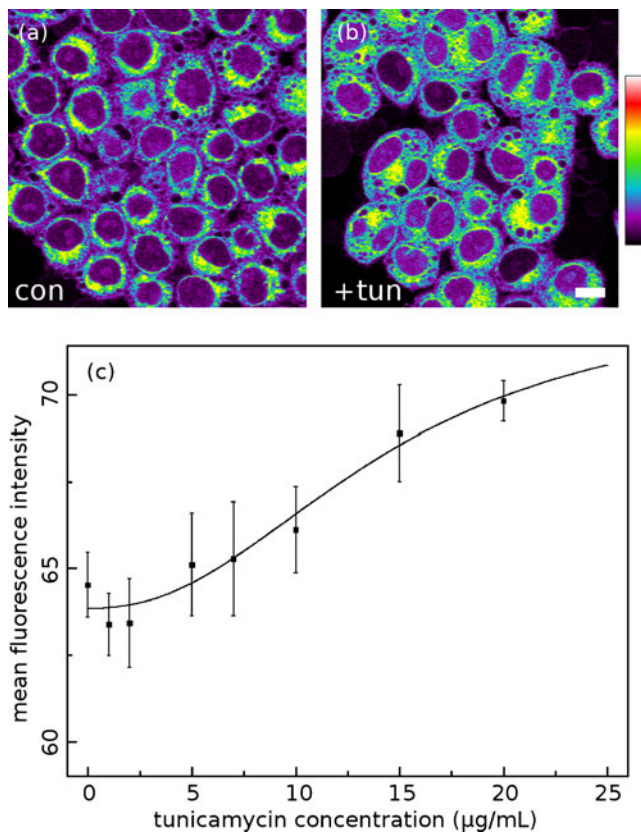


Fig. 7 HeLa cells treated with 20 µg/mL of tunicamycin and fixed (**b**) exhibit a higher level of ANS fluorescence than untreated fixed cells (**a**). The mean intensities of each thresholded image are plotted as a function of tunicamycin concentration, showing the dose–response relationship between ANS fluorescence and ER stress. A normalized response curve (for EC50) is overlaid (**c**)

protein synthesis and degradation. Care should be taken in the interpretation of ANS fluorescence images because of this constitutive, baseline level of ANS binding under unstressed conditions.

Changes in ANS fluorescence from this normal baseline reflect changes in the intracellular environment which change—usually increase—the number and hydrophobicity of ANS binding sites. Local thermal lesioning produces nonnatively folded protein that is readily detected by increased ANS fluorescence; the presence of unfolded protein at these lesion sites was confirmed by the simultaneous recruitment of the chaperone protein Hsp70. Multiphoton imaging of ANS fluorescence identifies specific regions subjected to thermal damage.

In contrast, the more general insult of whole-cell hyperthermia generates increases in ANS fluorescence at specific sites within the cell, particularly the nucleus and nucleolus. Accumulation of nucleolar ANS fluorescence suggests a target for further investigation, and elevated nucleolar ANS fluorescence is a readily visible marker for cell stress.

Interestingly, it has been reported that proteasome inhibition with MG132 triggers the accumulation of nuclear proteasomes in the nucleolus (Mattsson et al. 2001). Proteasome inhibition also causes the translocation to and accumulation of p53 in the nucleolus (Klibanov et al. 2001). Meanwhile, hyperthermia-driven nucleolar accumulation of Hsp70 is reduced by phosphoinositide 3-kinase and MEK inhibition. These findings, coupled with our results, bolster the view that the nucleolus is a sensitive signaling and sensing platform through which the cell can detect and respond to stress (Bański et al. 2010a, b).

In addition to direct damage to folded protein through thermal stress, we examined two other routes to an increased unfolded protein burden. Interfering with proper protein synthesis (by tunicamycin treatment, which causes ER stress and triggers the UPR by inhibiting glycosylation) drove a general increase in ANS fluorescence. Interfering with protein recycling (by MG132 treatment, causing inhibition of the 26S proteasome) stresses cells by preventing the degradation of damaged proteins and defective ribosomal products. MG132 treatment also inhibited the recovery of cells from the insult of thermal damage.

Practical applications of ANS fluorescence imaging

We foresee a number of applications for multiphoton ANS fluorescence imaging. This compound appears to have a low inherent toxicity in tissue culture, and it crosses intact, living cell membranes. We believe that it has great potential for use as a noninvasive marker for protein-damaging stress. If this low toxicity extends to multicellular organisms, ANS imaging may be useful in the *in vivo* study of microscopy-compatible model systems like *Caenorhabditis elegans*, embryonic zebrafish, *Xenopus*, and larval *Drosophila*.

For example, in *C. elegans* models of Aβ42 toxicity, it has been shown that knockdown of signaling proteins involved in protein homeostasis pathways can modulate Aβ42 pathology (Cohen et al. 2006); this study followed an individual molecular marker, Aβ42 immunofluorescence. ANS fluorescence imaging of this animal model could show whether alterations in protein homeostasis precede or occur concurrently with Aβ42 deposition, revealing where different proteostatic rescue mechanisms intervene in the Aβ42 aggregation pathway. The use of ANS fluorescence imaging in these types of applications will depend on a clear change in signal relative to background over the course of the experimental treatments. To this end, the nuclei of unstressed cells display a very low intrinsic ANS fluorescence. We have found that hyperthermia and proteasome inhibition, both of which affect protein homeostasis, elicit clear and measurable increases in nuclear ANS fluorescence. We therefore anticipate that monitoring

nuclear fluorescence may offer the most robust sensor for changes in protein homeostasis.

Live-cell ANS fluorescence imaging is useful for real-time kinetic experiments, but has the drawback of the high background fluorescence of serum-containing tissue culture media. For endpoint analysis, using formalin-fixed cells eliminates the need for culture medium (with its associated ANS binding and fluorescence) and allows samples to be stored and imaged later. ANS fluorescence imaging is compatible with cross-linking fixatives like formaldehyde only, as fixation with organic solvents like ethanol induces general protein denaturation and subsequent exposure of ANS binding sites (data not shown). While live-cell imaging requires the use of multiphoton fluorescence excitation to avoid ultraviolet-induced phototoxicity, we anticipate that fixed cells should be more resistant to photodamage caused by ultraviolet exposure. It may therefore be possible to perform limited ANS fluorescence imaging in fixed specimens using conventional confocal microscopy with excitation wavelengths between 350 and 405 nm. We have noted that ANS-stained samples photobleach very rapidly when exposed to ultraviolet light, making epifluorescence ANS microscopy unfeasible.

We were also able to use ANS in fixed, frozen tissue sections, which opens the door to the use of ANS fluorescence for endpoint analyses of stored or archived cells and tissues. ANS fluorescence imaging is not compatible with sections from paraffin-embedded tissue blocks because the deparaffinization process employs protein-denaturing solvents. Upsets to protein homeostasis and the accumulation of misfolded proteins have long been known to drive a host of human neurodegenerative diseases, including Alzheimer's, Parkinson's, amyotrophic lateral sclerosis, and Huntington's disease. While ANS is not superior to existing stains like thioflavin S for imaging amyloid deposits, it has a broader sensitivity to deposits composed of non-amyloid misfolded protein deposits such as Rosenthal fibers.

Recent work has focused on changes in protein homeostasis in malignant transformation (Moenner et al. 2007; Powers et al. 2009) where protein deposition is not a common pathological feature. We anticipate that ANS imaging can play a role in this area of research. For example, the uncontrolled proliferation of malignant cells places a heavy burden on the chaperone system to deal with increased rates of protein synthesis. A number of Hsp90 inhibitors that deprive malignant cells of this chaperone's protective function are now in clinical trials. High-throughput microscopy employing ANS fluorescence could be used to identify novel compounds that reduce chaperone activity in cell-based assays. These represent but a few of the possible applications for ANS fluorescence microscopy.

Acknowledgments The authors thank Suganthini Ilaalagan, Jennifer Glen, and Takyee Tung for the assistance in acquiring and for sectioning human brain tissue. We also greatly appreciate the efforts of Cheryl Hawkes in preparing and sectioning murine brain tissue. We thank Vikram Mulligan, Rishi Rakhit, and Nancy F.L. Ng for their helpful suggestions in preparing this manuscript. This research was funded in part by a grant from the Canadian Institutes for Health Research (AC) and by the Ontario Ministry of Health and Long Term Care. The views expressed do not necessarily reflect those of the OMOHLTC.

References

- Alastalo T, Hellesuo M, Sandqvist A, Hietakangas V, Kallio M, Sistonen L (2003) Formation of nuclear stress granules involves HSF2 and coincides with the nucleolar localization of Hsp70. *J Cell Sci* 116:3557–3570
- Balch WE, Morimoto RI, Dillin A, Kelly JW (2008) Adapting proteostasis for disease intervention. *Science* 319:916–919
- Bański P, Kodiha M, Stochaj U (2010a) Chaperones and multitasking proteins in the nucleolus: networking together for survival? *Trends Biochem Sci* 35:361–367
- Bański P, Mahboubi H, Kodiha M, Shrivastava S, Kanagaratham C, Stochaj U (2010b) Nucleolar targeting of the chaperone Hsc70 is regulated by stress, cell signaling, and a composite targeting signal which is controlled by autoinhibition. *J Biol Chem* 285:21858–21867
- Barrow CJ, Zagorski MG (1991) Solution structures of beta peptide and its constituent fragments: relation to amyloid deposition. *Science* 253:179–182
- Borrelli MJ, Bernock LJ, Landry J, Spitz DR, Weber LA, Hickey E, Freeman ML, Corry PM (2002) Stress protection by a fluorescent Hsp27 chimera that is independent of nuclear translocation or multimeric dissociation. *Cell Stress Chaperones* 7:281–296
- Brodsky JL, McCracken AA (1999) ER protein quality control and proteasome-mediated protein degradation. *Semin Cell Dev Biol* 10:507–513
- Cheung JC, Deber CM (2008) Misfolding of the cystic fibrosis transmembrane conductance regulator and disease. *Biochemistry* 47:1465–1473
- Chishti MA, Yang DS, Janus C, Phinney AL, Horne P, Pearson J, Strome R, Zuker N, Loukides J, French J, Turner S, Lozza G, Grilli M, Kunicki S, Morissette C, Paquette J, Gervais F, Bergeron C, Fraser PE, Carlson GA, George-Hyslop PS, Westaway D (2001) Early-onset amyloid deposition and cognitive deficits in transgenic mice expressing a double mutant form of amyloid precursor protein 695. *J Biol Chem* 276:21562–21570
- Chiti F, Dobson CM (2006) Protein misfolding, functional amyloid, and human disease. *Annu Rev Biochem* 75:333–366
- Choquet CG, Patel GB, Beveridge TJ, Sprott GD (1992) Formation of unilamellar liposomes from total polar lipid extracts of methanogens. *Appl Environ Microbiol* 58:2894–2900
- Cohen E, Bieschke J, Perciavalle RM, Kelly JW, Dillin A (2006) Opposing activities protect against age-onset proteotoxicity. *Science* 313:1604–1610
- Delom F, Emadali A, Cocolakis E, Lebrun J, Nantel A, Chevet E (2007) Calnexin-dependent regulation of tunicamycin-induced apoptosis in breast carcinoma MCF-7 cells. *Cell Death Differ* 14:586–596
- Denk W, Strickler JH, Webb WW (1990) Two-photon laser scanning fluorescence microscopy. *Science* 248:73–76
- Dyckman J, Weltman JK (1970) A morphological analysis of binding of a hydrophobic probe to cells. *J Cell Biol* 45:192–197

- Finegold L, Baker EA, Epel D (1974) Sea urchin egg fertilization studied with a fluorescent probe (ANS). *Exp Cell Res* 86:248–252
- Folch J, Lees M, Sloane Stanley GH (1957) A simple method for the isolation and purification of total lipides from animal tissues. *J Biol Chem* 226:497–509
- Fourie AM, Sambrook JF, Gething MJ (1994) Common and divergent peptide binding specificities of Hsp70 molecular chaperones. *J Biol Chem* 269:30470–30478
- Greenspan P, Mayer EP, Fowler SD (1985) Nile red: a selective fluorescent stain for intracellular lipid droplets. *J Cell Biol* 100:965–973
- Gregersen N, Bross P, Vang S, Christensen JH (2006) Protein misfolding and human disease. *Annu Rev Genomics Hum Genet* 7:103–124
- Hawkes CA, McLaurin J (2009) Selective targeting of perivascular macrophages for clearance of beta-amyloid in cerebral amyloid angiopathy. *Proc Natl Acad Sci USA* 106:1261–1266
- Hazel DL, Newland AC, Kelsey SM (1999) Malignancy: granulocyte colony stimulating factor increases the efficacy of conventional amphotericin in the treatment of presumed deep-seated fungal infection in neutropenic patients following intensive chemotherapy or bone marrow transplantation for haematological malignancies. *Hematology* 4:305–311
- Hiss DC, Gabriels GA, Folb PI (2007) Combination of tunicamycin with anticancer drugs synergistically enhances their toxicity in multidrug-resistant human ovarian cystadenocarcinoma cells. *Cancer Cell Int* 7:5
- Kelényi G (1967) Thioflavin S fluorescent and Congo red anisotropic stainings in the histologic demonstration of amyloid. *Acta Neuropathol* 7:336–348
- Klibanov SA, O'Hagan HM, Ljungman M (2001) Accumulation of soluble and nucleolar-associated p53 proteins following cellular stress. *J Cell Sci* 114:1867–1873
- König K (2000) Multiphoton microscopy in life sciences. *J Microsc* 200:83–104
- Kotliarova S, Jana NR, Sakamoto N, Kurosawa M, Miyazaki H, Nekooki M, Doi H, Machida Y, Wong HK, Suzuki T, Uchikawa C, Kotliarov Y, Uchida K, Nagao Y, Nagaoka U, Tamaoka A, Oyanagi K, Oyama F, Nukina N (2005) Decreased expression of hypothalamic neuropeptides in Huntington disease transgenic mice with expanded polyglutamine-EGFP fluorescent aggregates. *J Neurochem* 93:641–653
- Lin JH, Walter P, Yen TSB (2008) Endoplasmic reticulum stress in disease pathogenesis. *Annu Rev Pathol* 3:399–425
- Mahalingam D, Swords R, Carew JS, Nawrocki ST, Bhalla K, Giles FJ (2009) Targeting Hsp90 for cancer therapy. *Br J Cancer* 100:1523–1529
- Mattsson K, Pokrovskaja K, Kiss C, Klein G, Szekely L (2001) Proteins associated with the promyelocytic leukemia gene product (PML)-containing nuclear body move to the nucleolus upon inhibition of proteasome-dependent protein degradation. *Proc Natl Acad Sci USA* 98:1012–1017
- Moenner M, Pluquet O, Bouche-careilh M, Chevet E (2007) Integrated endoplasmic reticulum stress responses in cancer. *Cancer Res* 67:10631–10634
- Nollen EA, Salomons FA, Brunsting JF, Want JJ, Sibon OC, Kampinga HH (2001) Dynamic changes in the localization of thermally unfolded nuclear proteins associated with chaperone-dependent protection. *Proc Natl Acad Sci USA* 98:12038–12043
- Nonaka T, Hasegawa M (2009) A cellular model to monitor proteasome dysfunction by alpha-synuclein. *Biochemistry* 48:8014–8022
- Picard D, Suslova E, Briand P (2006) 2-Color photobleaching experiments reveal distinct intracellular dynamics of two components of the Hsp90 complex. *Exp Cell Res* 312:3949–3958
- Powers ET, Morimoto RI, Dillin A, Kelly JW, Balch WE (2009) Biological and chemical approaches to diseases of proteostasis deficiency. *Annu Rev Biochem* 78:959–991
- Semisotnov GV, Rodionova NA, Razgulyaev OI, Uversky VN, Gripas' AF, Gilmanshin RI (1991) Study of the “molten globule” intermediate state in protein folding by a hydrophobic fluorescent probe. *Biopolymers* 31:119–128
- Sherman M, Multhoff G (2007) Heat shock proteins in cancer. *Ann NY Acad Sci* 1113:192–201
- Skehan P, Storeng R, Scudiero D, Monks A, McMahon J, Vistica D, Warren JT, Bokesch H, Kenney S, Boyd MR (1990) New colorimetric cytotoxicity assay for anticancer-drug screening. *J Natl Cancer Inst* 82:1107–1112
- Slavik J (1982) Anilinonaphthalene sulfonate as a probe of membrane composition and function. *Biochim Biophys Acta* 694:1–25
- Trepel J, Mollapour M, Giaccone G, Neckers L (2010) Targeting the dynamic Hsp90 complex in cancer. *Nat Rev Cancer* 10:537–549
- Tupling AR, Gramolini AO, Duhamel TA, Kondo H, Asahi M, Tsuchiya SC, Borrelli MJ, Lepock JR, Otsu K, Hori M, MacLennan DH, Green HJ (2004) Hsp70 binds to the fast-twitch skeletal muscle sarco(endo)plasmic reticulum Ca^{2+} -ATPase (SERCA1a) and prevents thermal inactivation. *J Biol Chem* 279:52382–52389
- Unni VK, Weissman TA, Rockenstein E, Masliah E, McLean PJ, Hyman BT (2010) In vivo imaging of alpha-synuclein in mouse cortex demonstrates stable expression and differential subcellular compartment mobility. *PLoS ONE* 5:e10589
- Welch WJ, Feramisco JR (1984) Nuclear and nucleolar localization of the 72,000-dalton heat shock protein in heat-shocked mammalian cells. *J Biol Chem* 259:4501–4513
- Wippold FJ, Perry A, Lennerz J (2006) Neuropathology for the neuroradiologist: Rosenthal fibers. *AJNR Am J Neuroradiol* 27:958–961
- Witz G, Sivak A, van Duuren BL (1973) Interaction of a hydrophobic fluorescent probe with mouse embryo fibroblasts. *Exp Cell Res* 81:139–142
- Wójcik C, DeMartino GN (2003) Intracellular localization of proteasomes. *Int J Biochem Cell Biol* 35:579–589
- Wu B, Hunt C, Morimoto R (1985) Structure and expression of the human gene encoding major heat shock protein Hsp70. *Mol Cell Biol* 5:330–341
- Zeng X, Bhasin S, Wu X, Lee J, Maffi S, Nichols CJ, Lee KJ, Taylor JP, Greene LE, Eisenberg E (2004) Hsp70 dynamics in vivo: effect of heat shock and protein aggregation. *J Cell Sci* 117:4991–5000